



Supplementary Information for

A stress recovery signaling network for enhanced flooding tolerance in
Arabidopsis thaliana

Elaine Yeung¹, Hans van Veen¹, Divya Vashisht², Ana Luiza Sobral Paiva³, Maureen Hummel⁴, Tom Rankenberg¹, Bianka Steffens⁵, Anja Steffen-Heins⁶, Margret Sauter⁷, Michel de Vries⁸, Robert Schuurink⁸, Jérémie Bazin⁹, Julia Bailey-Serres^{1,4}, Laurentius A.C.J. Voesenek¹, and Rashmi Sasidharan¹

- 1) Plant Ecophysiology, Institute of Environmental Biology, Utrecht University, Utrecht, The Netherlands
- 2) Gregor Mendel Institute of Molecular Plant Biology, Austrian Academy of Sciences, Vienna, Austria
- 3) Programa de Pós-Graduação em Genética e Biologia Molecular, Departamento de Genética, Universidade Federal do Rio Grande do Sul, Porto Alegre, Brazil
- 4) Department of Botany and Plant Sciences, Center for Plant Cell Biology, University of California, Riverside, California, USA
- 5) Plant Physiology, Philipps University, Marburg, Germany
- 6) Institute of Human Nutrition and Food Science, Christian-Albrechts-Universität zu Kiel, Kiel, Germany
- 7) Plant Developmental Biology and Plant Physiology, Christian-Albrechts-Universität zu Kiel, Kiel, Germany
- 8) Plant Physiology, Swammerdam Institute for Life Sciences, University of Amsterdam, Amsterdam, The Netherlands
- 9) IPS2, Institute of Plant Science-Paris Saclay (CNRS-INRA), University of Paris-Saclay, Orsay, France

Julia Bailey-Serres
Email: serres@ucr.edu

Rashmi Sasidharan
Email: R.Sasidharan@uu.nl

This PDF file includes:

Supplementary materials and methods
Figs. S1 to S8
Tables S1 to S2
Captions for movie S1
Captions for dataset S1

Other supplementary materials for this manuscript include the following:

Movie S1
Dataset S1

Supplementary Information Text

SI Materials and Methods

Dark Treatment

10-leaf stage plants were placed in a dark climate chamber (20°C, 70% relative humidity) with well-maintained watering. After 5 d, plants were replaced in short-day light conditions.

Ribo-seq Bioinformatics

Data analysis was performed on a Linux cluster and R using command line tools, Bioconductor R packages, and custom R scripts. Some scripts were adapted from a systemPipeR Bioconductor R package for Ribo-seq experiments (1,2). Adapters were trimmed from FASTQ files, and reads of 24 to 36 nt were mapped to the *Arabidopsis thaliana* Col-0 genome (TAIR10/Araport11) in combination with the Araport11 annotation (GFF3 file, obtained from araport.org) using the TopHat and Bowtie2 alignment algorithm (version 2.2.5) allowing 2 mismatches. For reads with multiple mapping, reads were first given priority to the transcriptome and also based on alignment quality score. Log₂ Fold Changes (log₂FC) and Benjamini-Hochberg-corrected P-values were calculated using Bioconductor R packages “edgeR” and “limma.” Only genes with more than 15 reads in at least one sample were included. First, libraries were normalized for size and compositional bias with TMM normalization (trimmed mean of M-values). A generalized linear model with a full factorial design of treatment (3 levels: control, submergence, and recovery) and accession (2 levels: Bay-0 and Lp2-6) was fitted to the TMM normalized read count data with a negative binomial distribution. Appropriate comparisons of the treatment, accession and interaction coefficients allowed the calculation of log₂FC and significance for specific treatments, accession-specific treatment responses (accession × treatment interaction) and treatment-independent differences between the accessions. An MDS plot was created with “plotMDS” function within “edgeR” Bioconductor R packages. Samples distance was determined from the top 2000 differing genes in each pairwise comparison. Scatterplots of log₂FC comparisons were plotted using custom plotting functions on R. Genes behaving similarly and differently in both accessions were separately clustered with fuzzy K-means clustering (R “cluster” library). RPKM values normalized for library composition (TMM, “edgeR”) were scaled so that for each gene, the average RPKM across all samples was zero and standard deviation was one. Scaled RPKM values were used for fuzzy K-means clustering using Euclidean distances metrics and a membership exponent of 1.2. Genes that best represent their cluster over the entire flooding period (Membership Score > 0.5) were used for visual representation of clustering output. These genes were tested for Gene Ontology (GO) enrichment using the “GOseq” Bioconductor package assuming a hypergeometric distribution and Benjamini-Hochberg-corrected P-values.

Electron Paramagnetic Resonance (EPR) Spectroscopy

3 intermediate leaves were harvested for each treatment (control, dark, and recovery following submergence) and immediately snapped frozen in liquid N₂ (62). 150 μL of 1 mM TMT-H spin probe dissolved in 1 mM EDTA was added to each sample. Samples were incubated in a 40°C water bath for 90 min. 20 μL of supernatant was drawn up in a capillary tube for measurements on a Bruker Elexsys E500 spectrometer using the “Xepr acquisition and processing suite” software (Bruker Corporation, Billerica, Massachusetts). Measurements were performed at room temperature with the acquisition parameters: modulation frequency 100 kHz, modulation amplitude 1.3 G, receiver gain 60 dB, time constant 81.92 ms, conversion time 40.11 ms, center field 3512.95 G, sweep width 66.8 G, sweep time 41.07 s, and attenuation 30 dB. A calibration curve for the EPR spectrometer measurement was obtained using a nitroxide radical TEMPO (2,2,6,6-tetramethyl-1-piperidinyloxy). Calculations from double integration of the low field peak yielded the limit of detection as 0.011 mmol/L and the limit of quantification as 0.038 mmol/L. The concentration of TMT radicals was calculated from the area of the double integration of the low-field peak, which was converted into TEMPO radical equivalents using the calibration curve. ROS concentration was calculated based on the TEMPO-equivalents and the Avogadro constant where 1 mol = 6.022×10^{23} radicals, normalized by dry weight.

Methyl Viologen Application on *rbohD-3* and Col-0

Plants were sprayed with methyl viologen (0, 10, 20 μM) containing 0.1% (v/v) Tween-20 immediately upon de-submergence, and at 30 min and 1 h of recovery. Control plants were sprayed with 0.1% (v/v) Tween-20 to account for detergent effects. Plants were sprayed with 200 μL of solution each time.

Comparison of Cuticle-Associated Genes

From a database of acyl-lipid metabolism genes (3), DEGs ($P_{\text{adj}} < 0.05$) were identified in the Ribo-seq dataset classified as part of pathways relating to cutin and suberin synthesis and transport; lipid trafficking; wax biosynthesis; and fatty acid synthesis, elongation, desaturation, and export from plastids. Identified DEGs were plotted on scatterplots for comparison of Bay-0 and Lp2-6 under the “*submergence comparison*,” “*recovery comparison*,” or “*combined response*.”

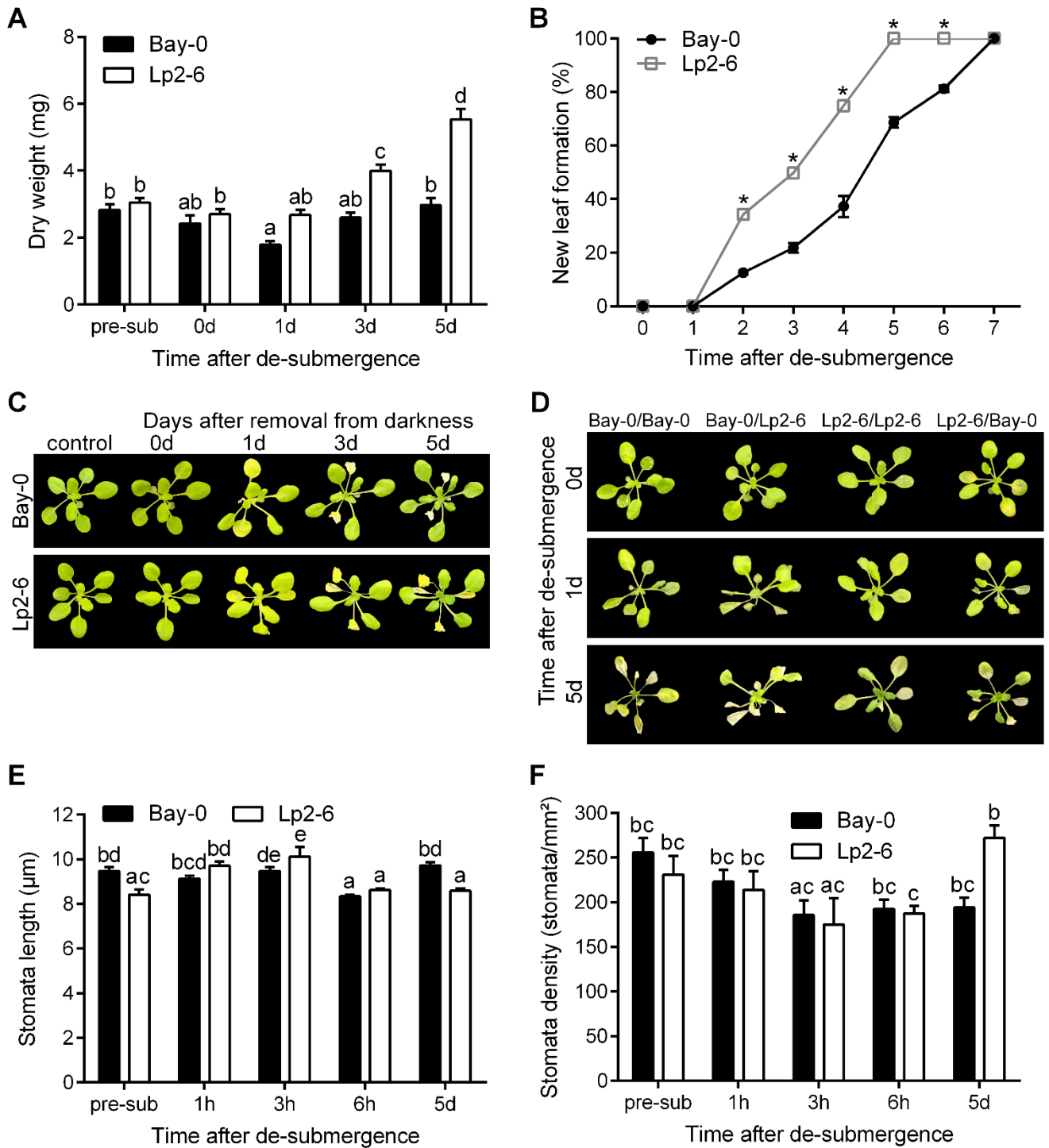


Fig. S1. Examining post-submergence recovery using a comparative *Arabidopsis* system. (A) Dry weight of whole rosettes during recovery after 5 d of dark submergence (n=9-10). (B) Percentage of plants forming new leaves during each day of recovery (n=32). Asterisks

represent significant difference between the two accessions at the specified time points ($p < 0.05$, two-way ANOVA). (C) Recovery of 10-leaf stage plants after 5 d of darkness as a control for dark submergence. (D) Representative images of grafted shoots after 5 d of submergence followed by recovery for 5 d. Images are shown for 0, 1, and 5 d of recovery. Sample groups represent the accession of the shoot/root. (E) Stomatal length measured on de-submerged intermediate leaves ($n=83-227$). (F) Stomatal density obtained from abaxial imprints of de-submerged intermediate leaves ($n=12-29$). Data represent mean \pm SEM. Different letters represent significant difference ($p < 0.05$, two-way ANOVA with Tukey's multiple comparisons test).

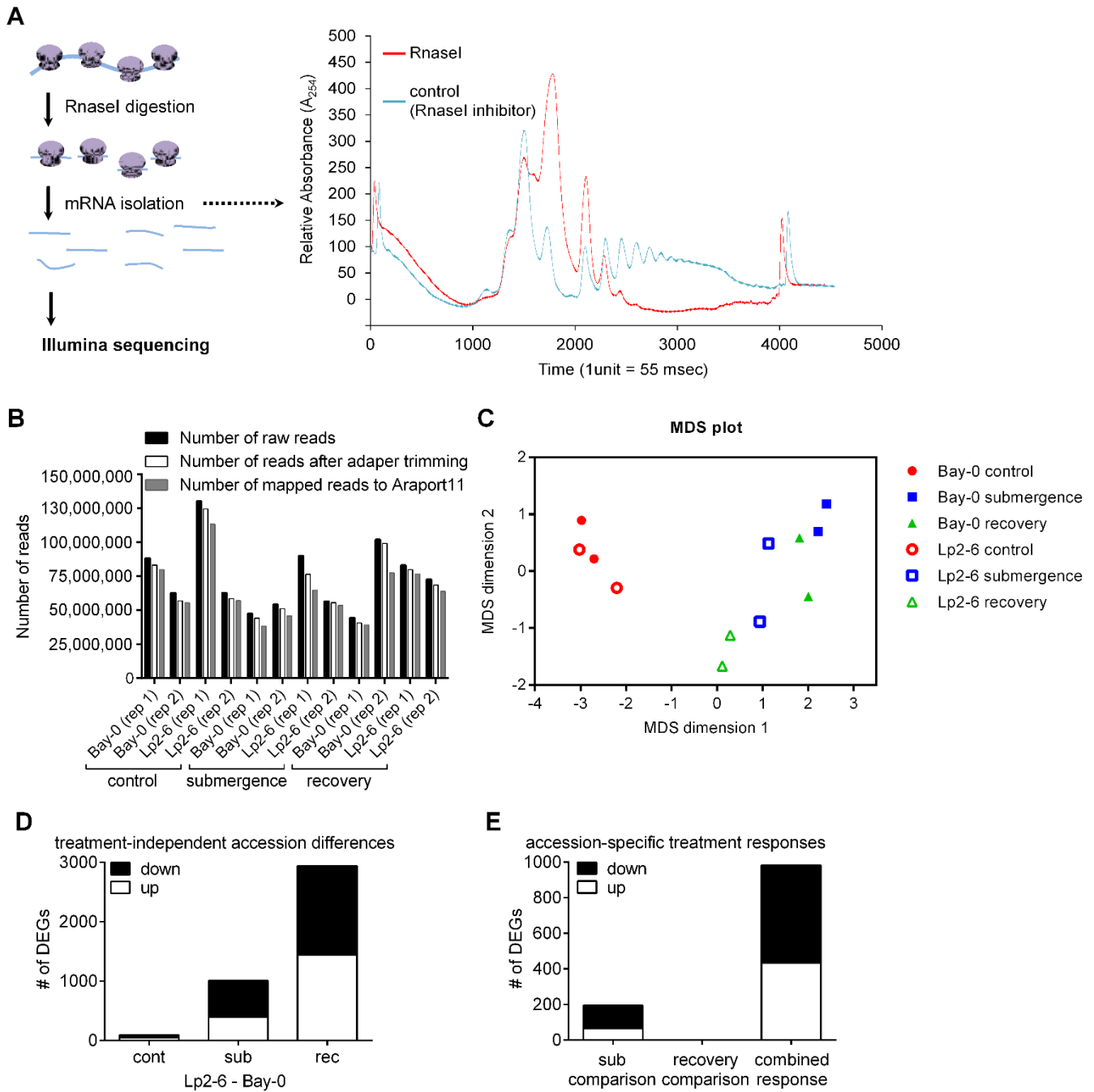


Fig. S2. Ribo-seq pipeline for identifying post-submergence molecular mechanisms. (A) Representative 254 nm absorbance spectra of sucrose density gradient fractionated control (undigested) and RNase I digested polysomes. The x-axis corresponds to the gradient, with the orientation of sedimentation shown. The first two peaks at the left represent the 40S and 60S monosomes, followed by the 80S peak and the denser polysome peaks. mRNA regions protected by ribosomes from digestion (ribosome footprints) were isolated and

constructed into cDNA libraries. (B) Illumina sequencing outputted high numbers of reads. Raw reads were unprocessed read output, trimmed reads were those with adapter sequences removed, and mapped reads were those aligning to the Araport11 Col-0 annotated genome. (C) Multidimensional scaling (MDS) plot showing distribution of the 2 biological replicates of air control, submergence, and recovery samples. Sample distances were calculated based on the top 2000 pairwise contrasting genes. (D) Number of differentially expressed genes (DEGs) ($P_{\text{adj}} < 0.05$) showing absolute differences independent of treatment responses, a comparison of Bay-0 and Lp2-6 read counts during the same treatment conditions. (E) Number of DEGs ($P_{\text{adj}} < 0.05$) showing accession \times treatment interaction effects for each comparison.

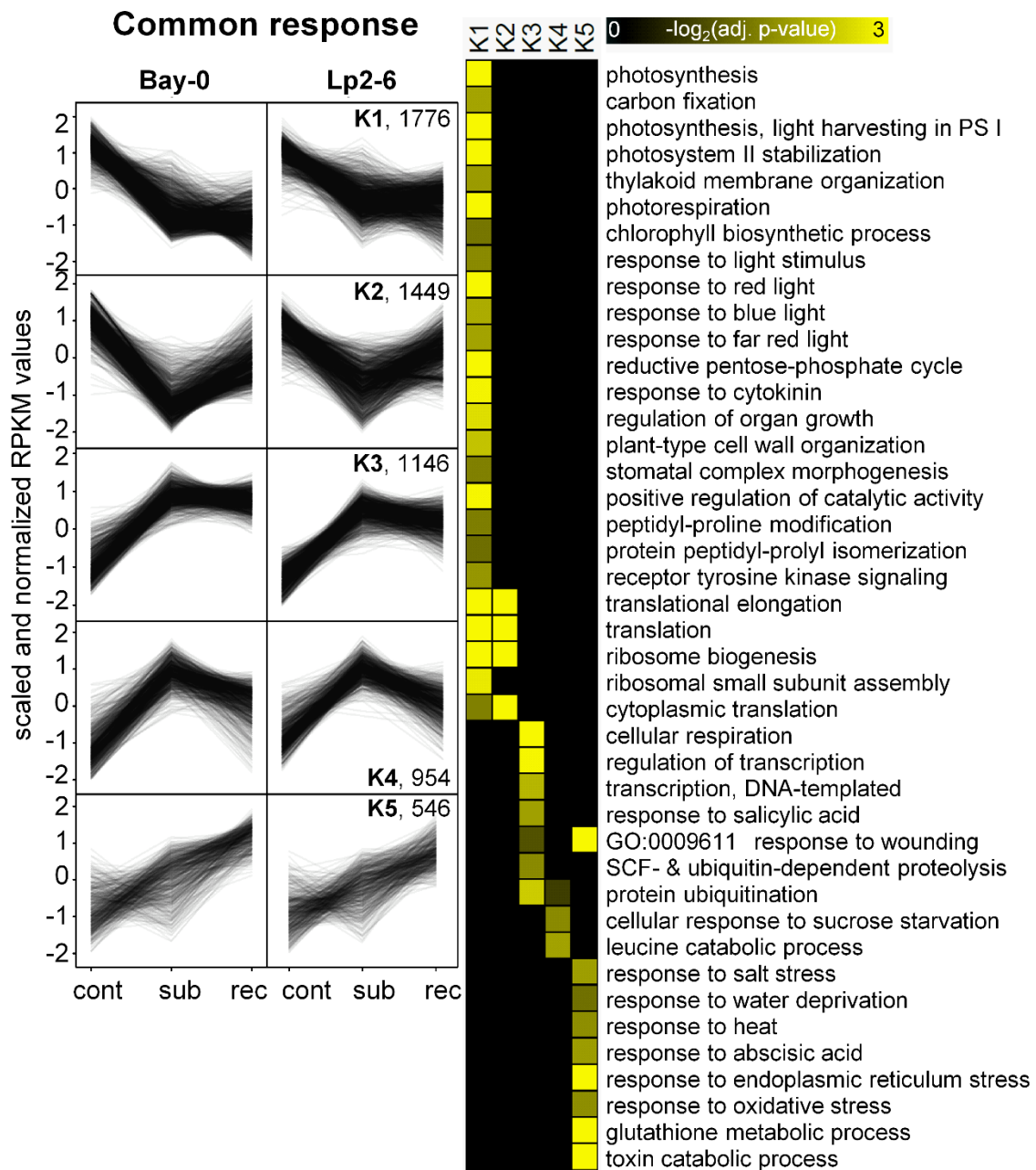


Fig. S3. Common molecular processes in Bay-0 and Lp2-6 after submergence and 3 h of recovery. Fuzzy K-means plots visualize the regulation patterns of common response DEGs ($P_{adj} < 0.05$) under control, submergence, and recovery. DEGs were individually plotted using RPKM values corrected for library size and library composition. GO analyses of identified clusters revealed associated biological processes, where higher yellow color intensity indicates a stronger correlation between the genes cluster and the GO term.

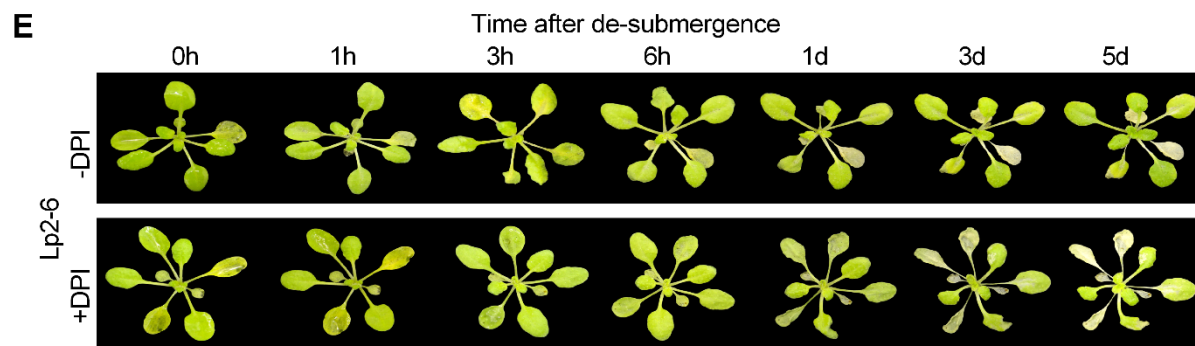
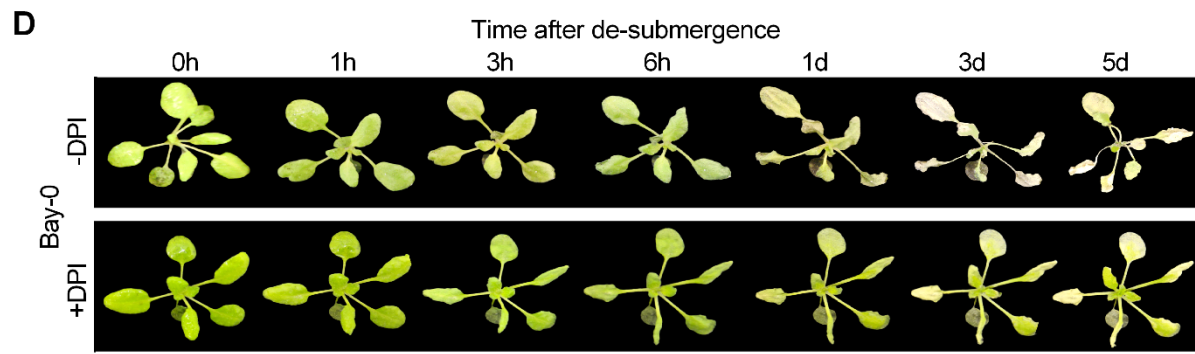
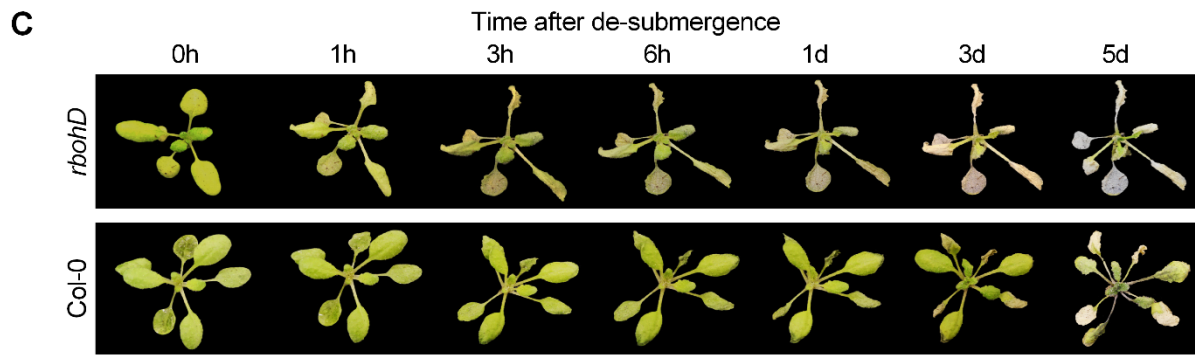
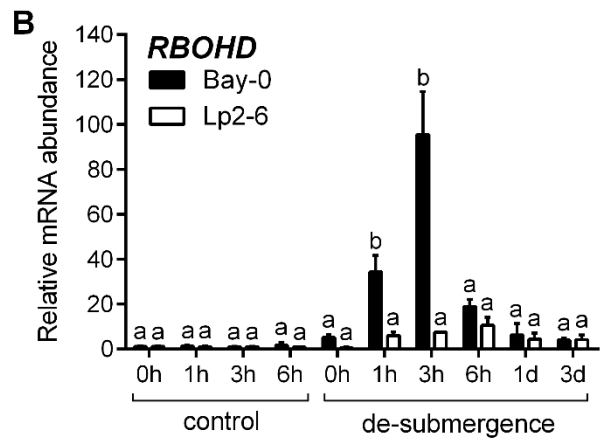
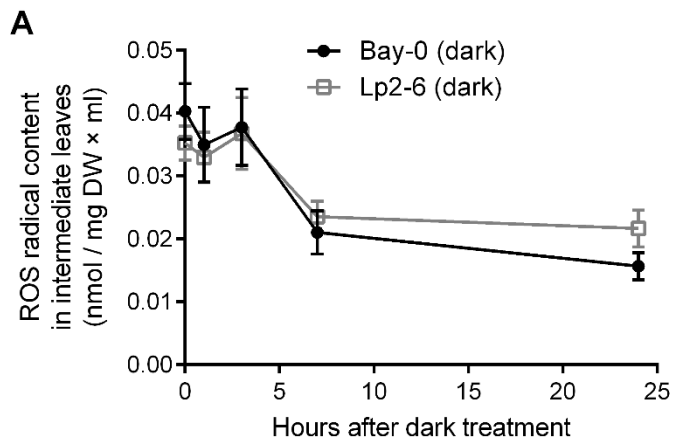


Fig. S4. Controlled ROS production is required for recovery signaling. (A) Electron paramagnetic resonance (EPR) spectroscopy quantified ROS in Bay-0 and Lp2-6 intermediate leaves of control or recovering plants after 5 d of darkness (n=30). There was no significant difference ($p < 0.05$) between the accessions at the specified time point. (B) Relative mRNA abundance of *RBOHD* measured by qRT-PCR in Bay-0 and Lp2-6 intermediate leaves following de-submergence after 5 d of submergence (n=3). Data represent mean \pm SEM. Different letters represent significant difference ($p < 0.05$, two-way ANOVA with Tukey's multiple comparisons test). (C) Representative images of *rbohD-3* mutants and Col-0 wild-type plants recovering after 6 d of dark submergence. Representative images of recovering Bay-0 (D) and Lp2-6 (E) plants sprayed with 200 μ M of the NADPH oxidase inhibitor DPI immediately upon de-submergence, following 5 d of submergence.

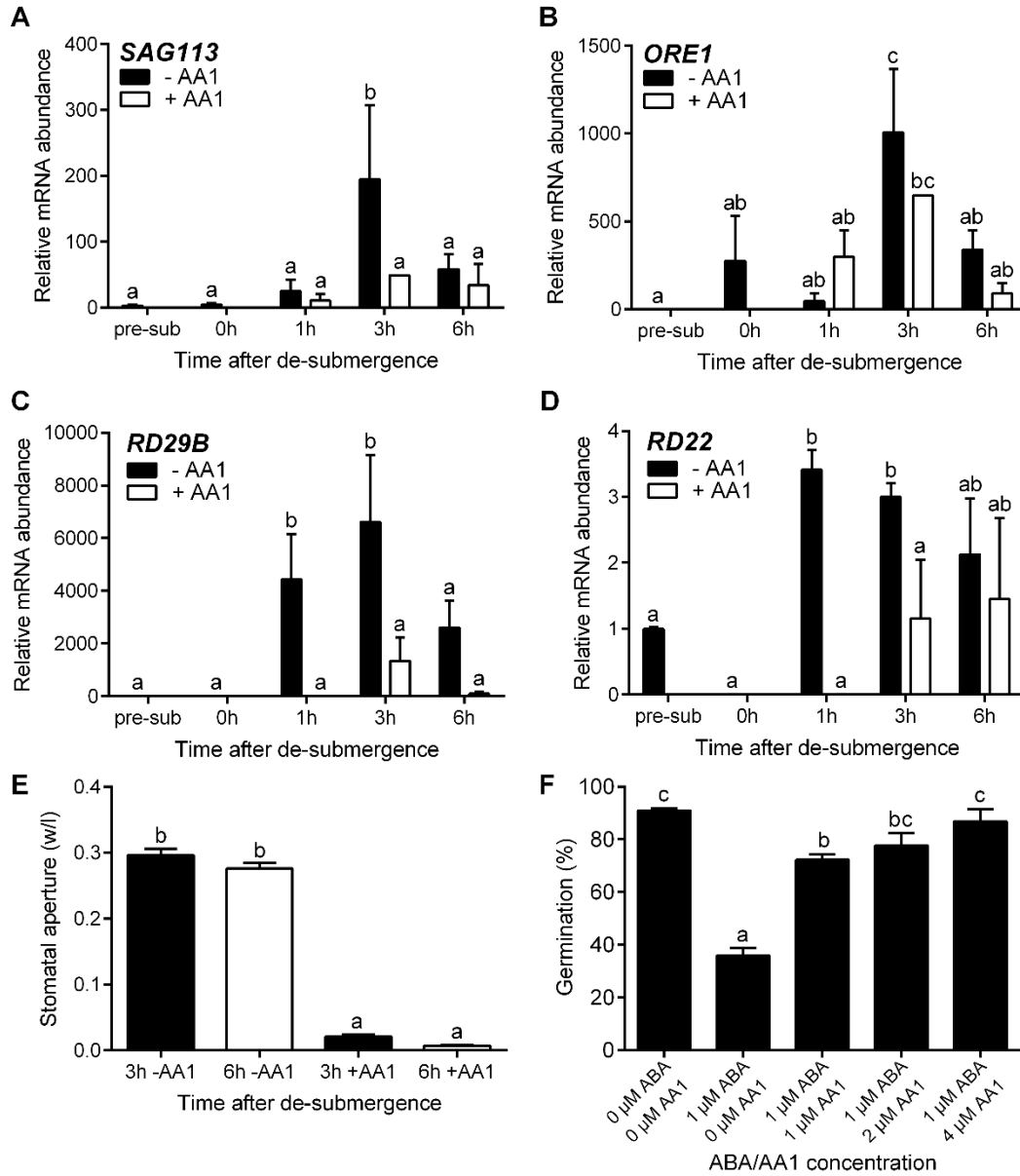


Fig. S5. ABA regulation of *SAG113* and *ORE1*. Relative mRNA abundance of *SAG113* (A), *ORE1* (B), *RD29B* (C), and *RD22* (D) measured by qRT-PCR in intermediate leaves of Bay-0 before treatment (pre-sub), after 5 d of submergence (0 h) and subsequent recovery and treated with or without AA1 (n=3-4). (E) Stomatal aperture (based on width/length ratio) for Bay-0 intermediate leaves with or without 100 μ M AA1 application upon de-submergence (n=300). (F) Seed germination rates of Col-0 on 1/2 MS medium with varying ABA and AA1 concentrations (n=5). Data represent mean \pm SEM. Different letters represent significant difference ($p < 0.05$, one- or two-way ANOVA with Tukey's multiple comparisons test).

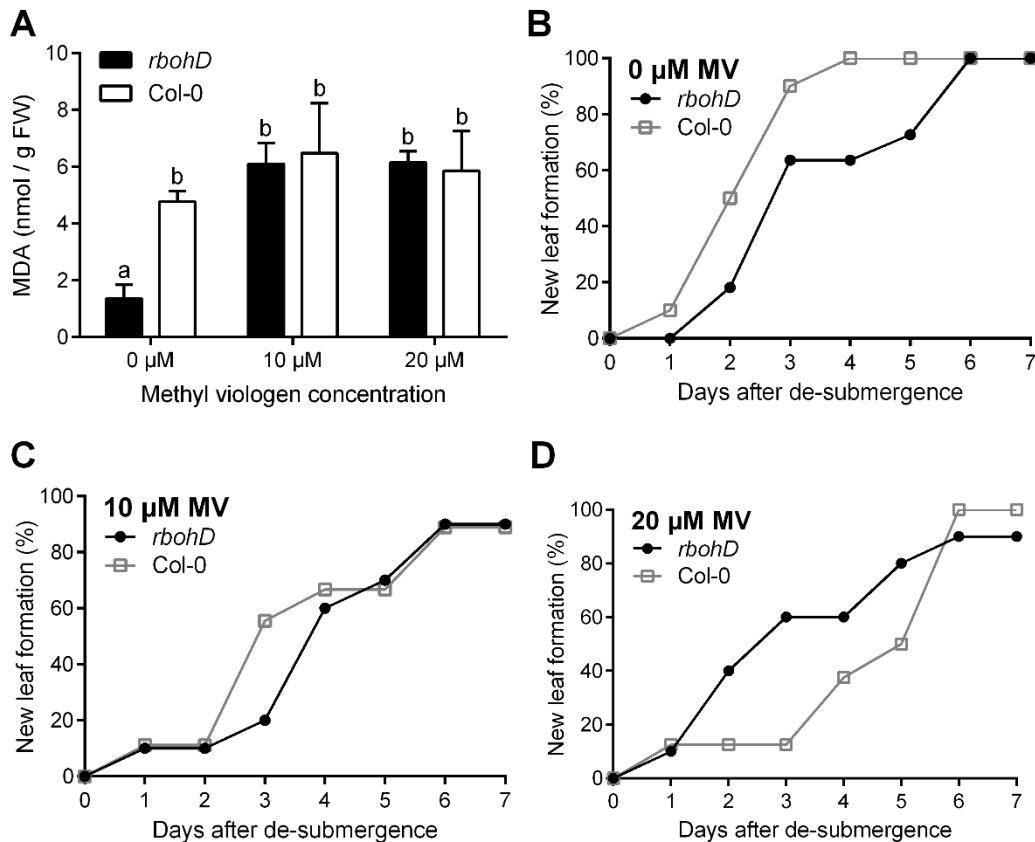


Fig. S6. Methyl viologen (MV) spraying on *rbohD-3* and Col-0 plants following de-submergence suggests that limited ROS production might be beneficial to recovery following 5 d of submergence. (A) Malondialdehyde (MDA) content of *rbohD-3* and Col-0 rosettes recovered for 1 d after spraying 0, 10, or 20 μM methyl viologen in the first hour upon de-submergence. Data represent mean \pm SEM (n=5). Significant difference is denoted by different letters ($p < 0.05$, two-way ANOVA with Tukey's multiple comparisons test). (B-D) New leaf formation of *rbohD-3* and Col-0 plants during recovery after spraying (B) 0 μM (n=10-11), (C) 10 μM (n=10), or 20 μM (n=8-10) methyl viologen upon de-submergence.

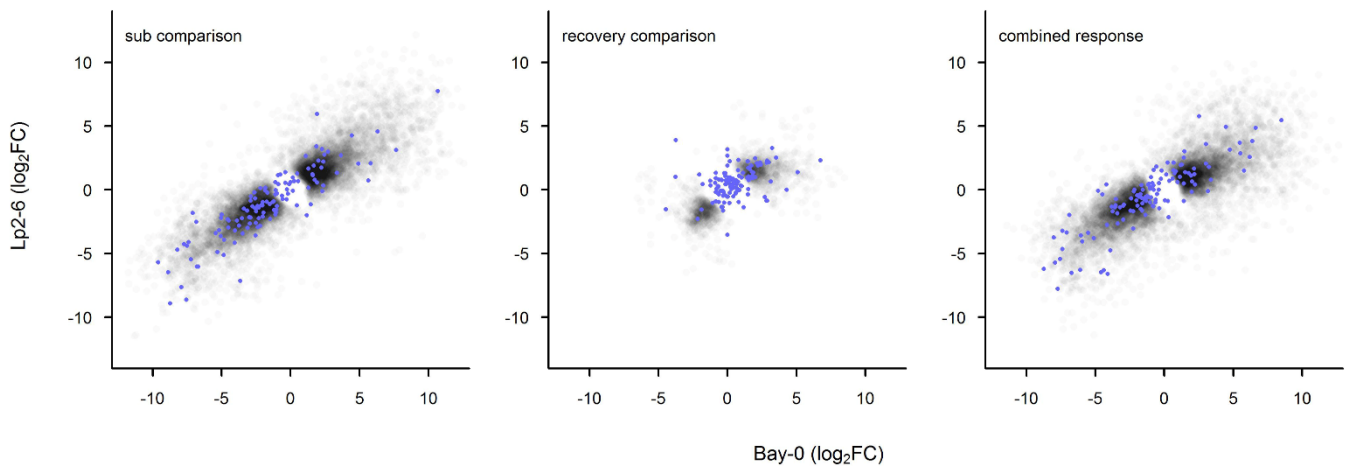


Fig. S7. Scatterplots comparing Bay-0 and Lp2-6 log₂FC under the “*submergence comparison*,” “*recovery comparison*,” and “*combined response*.” Black dots represent all DEGs (P_{adj}<0.05) in the Ribo-seq dataset and blue dots represent cuticular wax-related genes. Out of 123 cuticle/wax related DEGs, few DEGs exhibit an accession-specific difference under the “*submergence comparison*,” “*recovery comparison*,” or “*combined response*”: 31 DEGs (P_{adj}<0.05), 14 DEGs (P_{adj}<0.01), and 3 DEGs (P_{adj}<0.001).

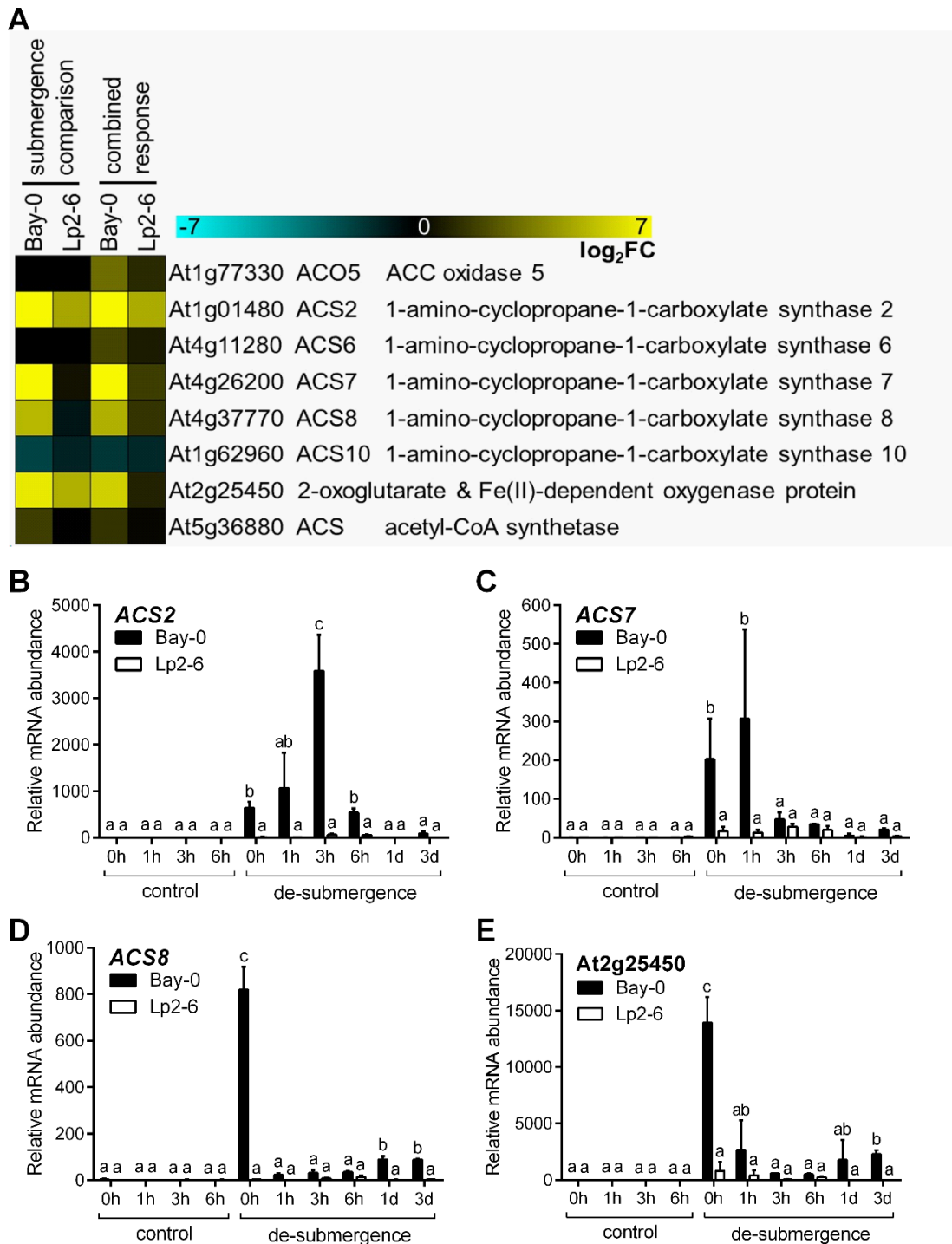


Fig. S8. Expression analysis data of genes encoding ACC synthase and ACC oxidase during submergence and upon de-submergence. (A) ACC synthase and ACC oxidase genes and related genes were identified in the Ribo-seq dataset. Genes with $P_{adj} < 0.05$ in Bay-0 or

Lp2-6 under the submergence or combined response comparison were displayed in a heat map. *ACC oxidase 5* (*ACO5*; AT1G77330), *ACC synthase 2* (*ACS2*; At1g01480), *ACS7* (At4g26200), *ACS8* (At4g37770), and a 2-oxoglutarate (2OG) and Fe(II)-dependent oxygenase superfamily protein (At2g25450; encoding a protein sequence similar to ACC oxidase) showed higher expression in Bay-0 compared to Lp2-6 under submergence and/or the combined response. (B-E) Relative mRNA abundance measured by qRT-PCR of (B) *ACS2*, (C) *ACS7*, (D) *ACS8*, and (E) At2g25450 in Bay-0 and Lp2-6 intermediate leaves following de-submergence after 5 d of submergence (n=3 biological replicates). Data represent mean \pm SEM. Different letters represent significant difference ($p < 0.05$, two-way ANOVA with Tukey's multiple comparisons test).

Table. S1. Primer sequences (5' → 3') for genotyping, indicated by the left primer (LP) and right primer (RP) of the insertion.

Mutant	ATG number	SALK/NASC Line	Sequence (5' → 3')
<i>sag113</i>	At5g59220	SALK_142672C	LP: TAATCGTCGTCCAGGTGTTG
			RP: TTTGACGATCACATGGCTGA
<i>ore1</i>	At5g39610	SALK_090154	LP: GATCTTAGGGTTACGTTGGGA
			RP: GGAAAGCCACAGGAAAAGAC
<i>rbohD-3</i>	At5g47910	N9555	LP: CGCCGAGACTCTCAAATTCA
			RP: ATACTGATCATAGGCGTGGC

Table. S2. Primer sequences (5' → 3') for qRT-PCR.

Gene	ATG number	Sequence (5' → 3')
<i>SAG113</i>	At5g59220	forward: TCGACGGTGA CTTACAGAGG
		reverse: GAGACTCGCATAGGACGACA
<i>ORE1</i>	At5g39610	forward: TCTGCTACTGCCATTGGTGAAGT
		reverse: TCGGGTATTTCCGGTCTCTCAC
<i>RBOHD</i>	At5g47910	forward: CCGGAGACGATTACCTGAGC
		reverse: CGTCGATAAGGACCTTCGGG
<i>RD29B</i>	At5g52300	forward: GAACGTCGTTGCCTCAAAGC
		reverse: TGCCCGTAAGCAGTAACAGATC
<i>RD22</i>	At5g25610	forward: CGGCTGATTTAACACCGGAG
		reverse: ACCTCCCTTTCCAACGTTCA
<i>ACS2</i>	At1g01480	forward: GGATGGTTTAGGATTTGCTTTG
		reverse: GCACTCTTGTTCTGGATTACCTG
<i>ACS7</i>	At4g26200	forward: ACGGTACGATAACCATTGTGGA
		reverse: GCTCGCCGTCTTTAGTTTTCT
<i>ACS8</i>	At4g37770	forward: TGGGTCTAGCAGAAAATCAGTTG
		reverse: TCCGACATGAAATCCGCCAT
	At2g25450	forward: TATGAGTCTCCTGCTGCGAG
		reverse: ATCTCCCCACAAACCTCAGG
<i>ACTIN2</i>	At3g18780	forward: TTCGTGGTGGTGA GTTTGTT
		reverse: GCATCATCACAAGCATCCTAA

Movie S1. Time-lapse of a representative Bay-0 and Lp2-6 rosette recovering in normal growth conditions after 5 d of dark submergence.

Additional dataset S1 (separate file)

Log₂FC, Benjamini-Hochberg-corrected P-values, and fuzzy K-means cluster number for all genes in the Ribo-seq dataset. Data is organized by 3 comparisons: submergence (plants submerged for 5 d in the dark compared to control plants), recovery (plants recovered for 3 h after de-submergence following 5 d of submergence compared to plants immediately de-submerged after 5 d of submergence), and combined response (plants recovered for 3 h compared to control plants).

References:

1. Backman TWH, Girke T (2016) systemPipeR: NGS workflow and report generation environment. *BMC Bioinformatics* 17:388.
2. Juntawong P, Bazin J, Hummel M, Bailey-Serres J, Girke T (2015) systemPipeR workflow for Ribo-seq and polyRibo-seq experiments. Available at www.bioconductor.org. Accessed January 1, 2018.
3. Li-Beisson, Y. *et al.* (2013) Acyl-lipid metabolism. *Arab. B.* 11, e0161